Int. J. Electrochem. Sci., 12 **(2017)** 1025 – 1033, doi: 10.20964/2017.02.27

International Journal of
ELECTROCHEMICAL
SCIENCE
www.electrochemsci.org

Sulfur/hollow Carbon Nanofiber Composite as Cathode Material for Lithium-Sulfur Batteries

Yan Yuan[*], *Zhao Fang, Manbo Liu*

School of Metallurgical Engineering, Xi'an University of Architecture and Technology, Xi'an 710055
[*]E-mail address: lingyi21@126.com

Received: 7 November 2016 / *Accepted:* 11 December 2016 / *Published:* 30 December 2016

Hollow carbon nanofiber was selected as the conductive matrix for elemental sulfur. The influences of preparation method and sulfur content on the structure and properties of the composite were investigated. It is found that the treatment process is inclined to produce large-sized sulfur particles accompanied by severe agglomeration. On the contrary, uniform distribution and compact contact can be established between sulfur and carbon for the composite based on liquid phase precipitation and appropriate sulfur content. The hollow nanofiber material with superior conductivity, abundant holes and good mechanical property, constructs a highly-conductive, porous and stable three-dimensional framework, promoting the electrochemical performances of lithium sulfur batteries.

Keywords: sulfur carbon composite; hollow carbon nanofiber; liquid phase precipitation; lithium sulfur battery; electrochemical performance

1. INTRODUCTION

Lithium-sulfur (Li-S) batteries [1] have been considered to be one of the most promising energy storage systems, owing to its high energy density, low material cost and favorable environmental friendliness. Its application in the fields of electric vehicles would be of great significance for the energy conservation and environmental protection around the world. However, the commercialization of the battery has been severely restricted by the problems below. On the one hand, the insulation of the elemental S leads to low utilization of active material and weak rate capability. On the other hand, the dissolution and shuttle of intermediates-polysulfides [2] cause rapid capacity fading and self-discharge issues.

Cathode is a primary component for Li-S batteries. In recent years, various conductive carbons [3] have been chosen to combine with elemental S, such as active carbon, carbon nanofiber and

graphene [4-6], with the purpose of enhancing conductivity of cathode, maintaining the stability of cathode structure and inhibiting dissolution of polysulfides. Especially, hollow carbon nano-materials with large specific surface area and abundant holes have been attempted to develop advanced Li-S batteries. For instance, Brun et al. [7] synthesized hollow carbon spheres by a hydrothermal carbonization procedure in the presence of monosaccharide as carbon precursor and silica nanoparticle as hard template. The fabricated S/C composite owns outstanding cycle and rate properties due to the unique nanostructure of the hollow spheres. Chen et al. [8] reported a hierarchical architecture S/MWCNT nano-microsphere with large hollow pores, prepared through a solvent exchange and further ball-milling strategy, which also exhibits excellent electrochemical performances.

Herein, a kind of novel hollow carbon nanofiber (HCF) was chose as the conductive matrix for loading S. This one-dimensional hollow material not only favors better electron conduction and ion diffusion, but also provides a stable framework for holding cathode structure and sufficient deposition positions for insoluble products. In this paper, different preparation methods and S content of the S/HCF composite were compared, and the effects of material composition and morphology on electrochemical properties were investigated. Especially, the mechanism or reason on improving cell performances via the HCF was intensively discussed.

2. EXPERIMENTAL

2.1 Composite preparation

The S/HCF composite was prepared by a liquid precipitation route as follows: 12.408g sodium thiosulfate ($Na_2S_2O_3$) was dissolved in 250ml deionized water containing polyethylene glycol (PEG, M_w=400) as dispersant. Then, the HCF (Aldrich) was dispersed ultrasonically for 1h and stirred magnetically for 30min in above mixture to form solution A (the mass ratio of S to HCF is 7:3 in theory). Then 2 mol L^{-1} formic acid solution containing PEG was served as solution B. The S/HCF composite continuously formed when solution A was added slowly into solution B under magnetic agitation state. After reaction, the product was separated centrifugally from the obtained suspension, washed by ethanol and deionized water several times, and finally dried at 60℃ in a vacuum oven for 48h (marked as LSC73). Another composite material was prepared by the same process above, with a mass ratio of S to HCF at 8:2 in theory (marked as LSC82).

For comparison, heat treatment method was also used for preparing the composite material: sublimed S (Alfa, 99.9%) was incorporated to the HCF by heating the S/C mixture (with a mass ratio of S to HCF at 7:3) at 155℃ for 12 h in an Ar–filled furnace at a heating rate of 5 ℃ min^{-1}. Then the system was cooled down to the room temperature. The obtained composite was collected and marked as HSC73.

2.2 Cathode fabrication and cell assembly

The composite cathode was fabricated by mixing 80 wt% composite, 10 wt% carbon black (Super P), and 10 wt% mixture of sodium carboxyl methyl cellulose (CMC) and styrene butadiene

rubber (SBR) (2:1 mass ratio). The resultant electrode was punched into circular disks with S loading of ~1.2 mg cm^{-2}.

The coin cells were assembled by sandwiching a porous polypropylene separator (Celgard 2400) between the as-prepared cathode and Li metal in an Ar-filled glove box. The electrolyte consisted of 1 mol L^{-1} lithium bis(trifluoromethanesulfonyl)imide (LiTFSI) in a solvent mixture of 1,2-dimethoxyethane (DME) and 1,3-dioxolane (DOL) (1:1, volume ratio).

2.3 Characterization and measurement

The crystalline phases of the samples were investigated via a powder X-ray diffraction system (XRD, Rigaku3014), using Cu Kα as the radiation source at a scan rate of 2° min^{-1}. Thermogravimetric analysis (TGA, SDTQ600) was conducted in testing the thermal stability of the composite under N_2 atmosphere at a heating rate of 5℃ min^{-1}. The morphologies of the materials and electrodes were observed by a field emission scanning electron microscopy (FESEM, Quanta FEG250). The element distributions of electrode surface were identified by energy dispersive X-ray spectroscopy (EDS).

The charge-discharge tests were carried out at a battery test system (CT2001A) between 1.5~3.0 V. The electrochemical impedance spectroscopy (EIS) was performed on an electrochemical workstation (M2273) in the frequency range of 10^5 Hz~0.1 Hz with an amplitude of ±5 mV. Cyclic voltammetry (CV) was also conducted using this workstation at a scan rate of 0.1 mV s^{-1}.

3. RESULTS AND DISCUSSION

XRD patterns of various samples are shown in Fig. 1a. Elemental S belongs to orthorhombic type (S8, JCPDS#08 0247), which is stable at room temperature. HCF exhibits a partially-graphitized and amorphous structure with one broad and low intensity peak at ~26°, ascribing to (002) diffraction peak of carbon [9]. Three composites all have plenty of sharp diffraction peaks in the whole range, with the highest peak at ~23° (representing (222) crystal plane of S [9]). It confirms the existence of S crystals in the composite. The similar peak intensities occur between these composites and elemental S, implying that a part of S particles may be formed on the surface of HCF [10].

Fig. 1b presents the results obtained from TGA tests on the as-prepared composites. The weight loss of LSC73, HSC73 and LSC82 are continuous from 150℃ until they are heated to over 310℃, 280℃, 275℃, dropping to 32%, 31.8%, 23.5%, respectively. Since HCF is stable in the above temperature range, the decline in composite weight is mainly attributed to phase transformation of elemental S. The S on the surface of HCF begins to evaporate at first, and then the evaporation expands to S inside the carbon pores. Finally, the CNF is responsible for all of the residual weight. Hence, the S content in the three composites reaches 68 wt%, 68.2 wt% and 76.5 wt%, respectively. The thermal stability of LSC73 is significantly better than HSC73 and LSC82 because of its slowest weight loss. The weight loss rate is always related to the location of S within the carbon matrix [11], which can be used for evaluating the combination force between S and C. Low weight loss rate means

that high adsorption energy needs to be overcome for S evaporation [11]. It seems that S adheres to carbon matrix more closely in LSC73 than in the other two composites, probably ascribing to deeper penetration of S into the carbon pores.

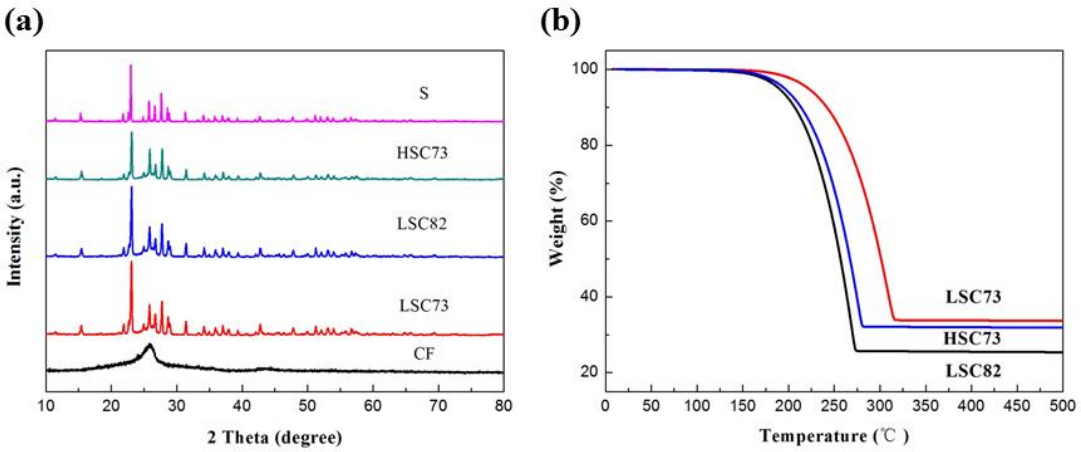

Figure 1. (a) XRD patterns and (b) TGA curves of different S/HCF composites

Fig. 2 shows the morphological characterization of the HCF. It can be seen from Fig. 2a that HCF has good one-dimensional nanofiber structure, with approximately 100~250 nm in diameter. The fibers intertwine with each other to create a complicated network with plentiful holes. As shown in Fig. 2b, HCF is typically hollow inside the fiber wall, which is significantly different from conventional nanofiber materials [12, 13].

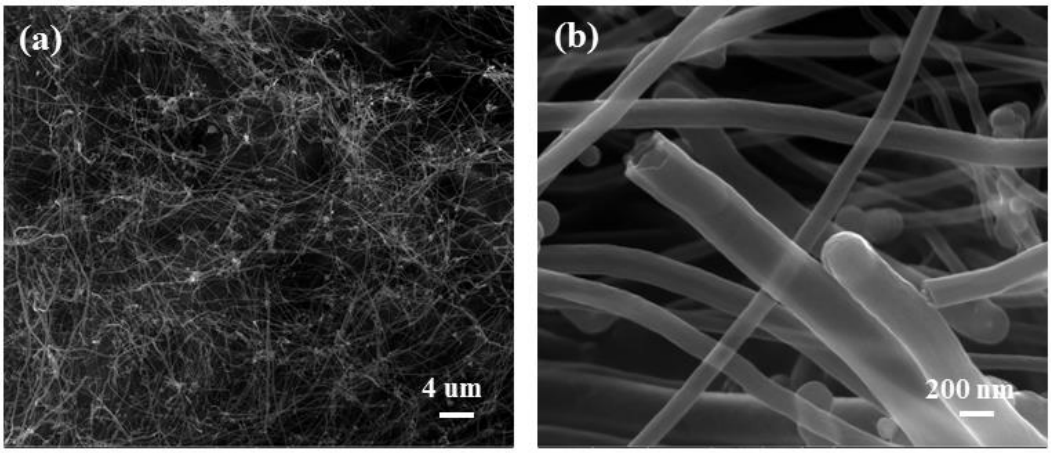

Figure 2. SEM images of HCF: (a) low-magnification; (b) high-magnification

SEM images of the as-prepared S/HCF composites were compared in Fig.3. For LSC73 (Fig.3a and 3b), plenty of S spherical particles are found to be located in the abundant voids formed by intertwining of the HCF, and the nanofibers wrap densely outside the particles in the net-like form,

establishing compact contact (or strong combination) between S and C. The EDS analysis (Fig.3c) discovers the S particles are dispersed uniformly in the whole HCF matrix. For HSC73 (Fig.3d and 3e), elemental S produces severe agglomeration with various irregular shapes. Most of the agglomerates reach tens of microns in size, far beyond the composites prepared via liquid phase deposition. At this moment, the distribution of S throughout the composite is quite inhomogeneous (as shown in Fig.3f). It would be attributed to the following two points. First of all, the elemental S and HCF may not achieve adequate dispersion in porcelain crucible before heat treatment, leading to uneven permeation of molten S into the HCF framework at high temperature. After that, secondary agglomeration could be initiated owing to the surface energy of particles during the cooling process. The SEM results are consistent with previous XRD and TGA tests.

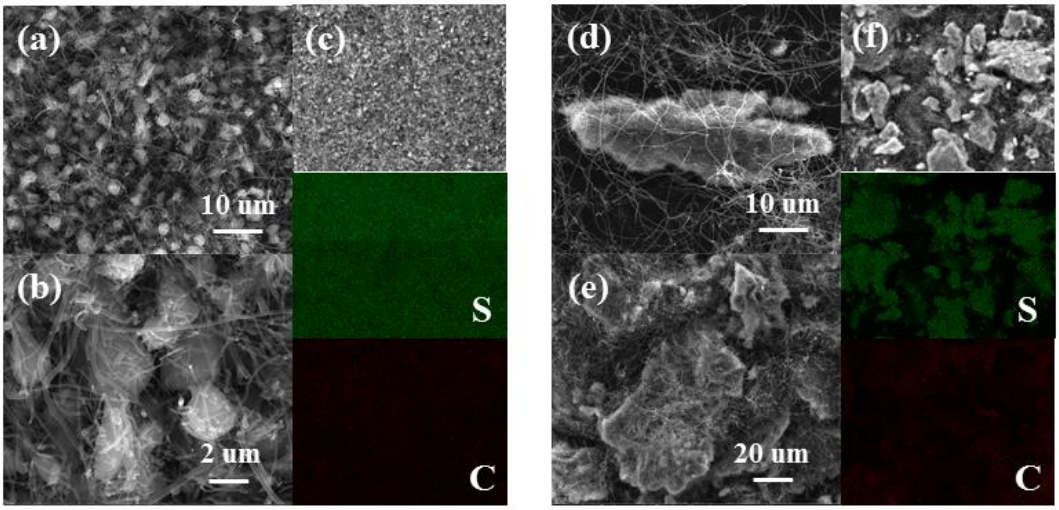

Figure 3. SEM images of (a, b) LSC73 and (d, e) HSC73; EDS mapping of (c) LSC73 and (f) HSC73

The electrochemical performances of different S/HCF composite cathodes were investigated and the results are presented in Fig.4. In CV curves (Fig.4a), two reduction peaks located at ~2.35 V and 2.0 V stand for the reduction of elemental S to soluble polysulfides and then to the insoluble Li_2S_2/Li_2S, respectively. Only oxidation peak at ~2.55 V represents the conversion of lithium sulfide into oxidized active S (Li_2S_8 or S) [14]. The positions of above peaks have almost no change during cycling, implying good redox reversibility. But the areas of reduction peaks greatly reduce after undergoing two cycles, which is mainly associated with the dissolution of polysulfides in the electrolyte. Then the reduction peaks overlap well at subsequent cycles. It means that polysulfides establish a dynamic balance between solid phase and liquid phase, thus the dissolution loss tends to stabilize gradually. The two potential plateaus in the discharge profiles of Fig. 4b reveal two steps of reduction reactions between S and Li, corresponding to the two reduction peaks in CV. It can be seen that the low-potential plateau is much longer than the high-potential one, thus the main contribution to discharge capacity comes from the conversion of polysulfides into Li_2S_2/Li_2S. It is noteworthy that the overcharge always occurs with cycles, reflecting inevitable shuttle issue for the electrolyte in absence of $LiNO_3$.

Fig.4c and 4d exhibits the cycle performances of the composite cathodes (the current density is 0.1 C). The initial capacity is relatively high in general for three cathodes (especially 1165 mAh g^{-1} for LSC73). The porous and conductive network constituted by HCF is convenient for infiltration of the electrolytes into the cathode and adequate charge transfer, thus providing plenty of active reaction points. The drastic capacity fading is observed in first two cycles due to the dissolution of polysulfides [15], but the capacity retention is acceptable in subsequent cycles, reaching 75.7%, 61.2%, 60.6% (according to second discharge capacity) for LSC73, LSC82, HSC73, respectively. The electrochemical property of LSC73 is relatively superior to that employing ordinary carbon fiber [13], which is benefited from the advantageous morphology and structure of the HCF and resultant composite. LSC82 cathode delivers low reversible capacity and poor cycle capability, even though it owns high S content. It is possible that a part of S particles are overloaded in this composite, and lack of good combination with HCF. Thus their contributions to capacity value are limited. Moreover, these overloaded S would be inclined to drop off from the cathode and lose electro-activity with cycles, causing irreversible capacity loss. As for HSC73, the low utilization of active material is comprehensible on account of the agglomeration issue. The cathode structure may be further deteriorated if undesired discharge products are further deposited on these massive particles.

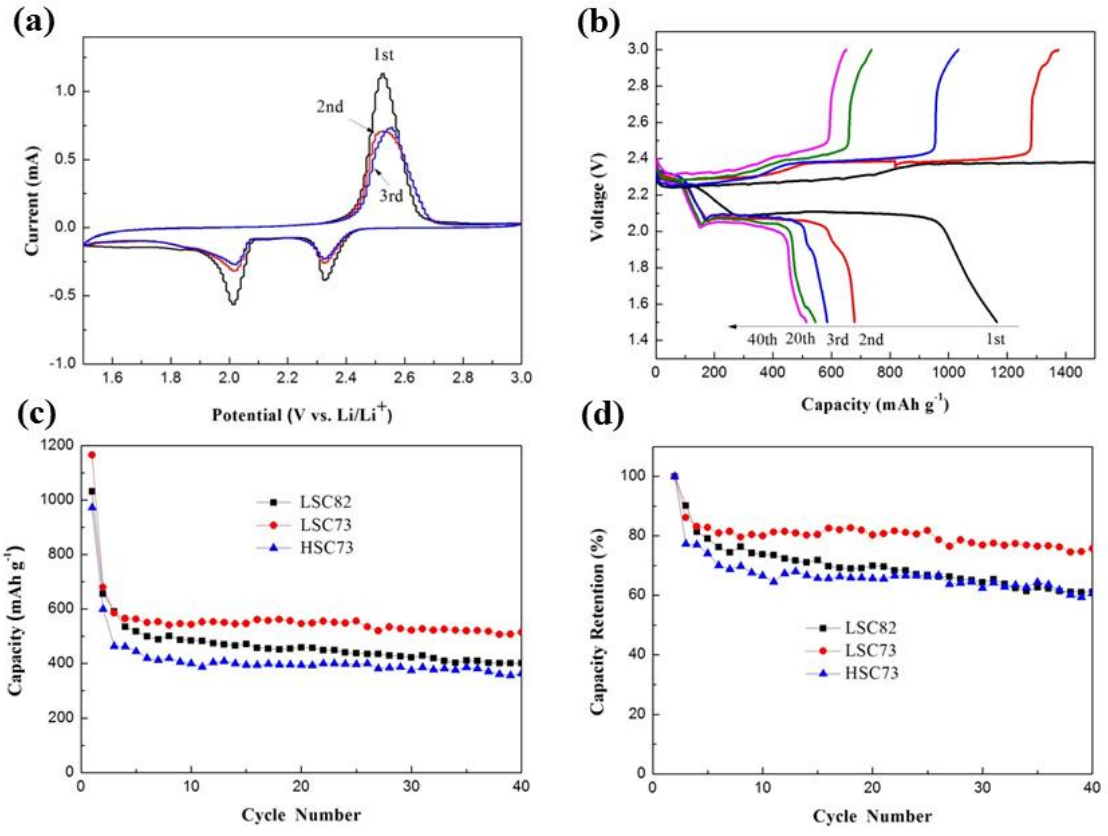

Figure 4. (a) CV curves and (b) potential profiles of LSC73 cathode; cycle performances of different S/HCF cathodes: (c) specific capacity for discharge; (d) capacity retention (according to the 2nd discharge capacity)

The impedance plots of various S/HCF composite cathodes were presented in Fig. 5. Before cycle, the plots are composed of a semicircle in high frequency and an inclined line in low frequency (Fig. 5a). The former refers to the interface charge-transfer resistance (R_{ct}), and the latter corresponds to Warburg impedance (W_o, reflecting Li^+ diffusion in the active material). The high-frequency intercept on the real axis represents the ohmic resistance (R_o), including the electrolyte and electrode resistances [16]. The lowest R_{ct} value for LSC 73 further illustrates that uniform distribution of S in the composite and close contact between S and C are beneficial to electrode conductivity and charge transfer within the electrode.

The impedance responses of LSC73 cathode at different cycle stages were shown in Fig. 5b. After cycles, the plots are divided into two obvious semicircles in high frequency. The additional semicircle is always related to Li^+ migration through the solid-electrolyte interface (SEI) film formed during the charge–discharge process (R_s) [16]. The fitted resistance data according to the equivalent circuit of Fig. 5c are summed in Fig. 5d. The effect of polysulfides dissolution on electrolyte resistance seems to be limited due to the slight change in R_0 with cycles. The gradual increase in R_s means that denser and thicker SEI would be formed considering the deposition of insoluble products on the electrode. The drastic decline of R_{ct} after cycling is probably attributed to the redistribution of S in the HCF matrix and the penetration of the electrolyte into the electrode [17]. The resistance value remains relatively stable at subsequent cycles. It is benefited from the highly-conductive and porous three-dimensional network constructed by the unique hollow carbon nanofiber material.

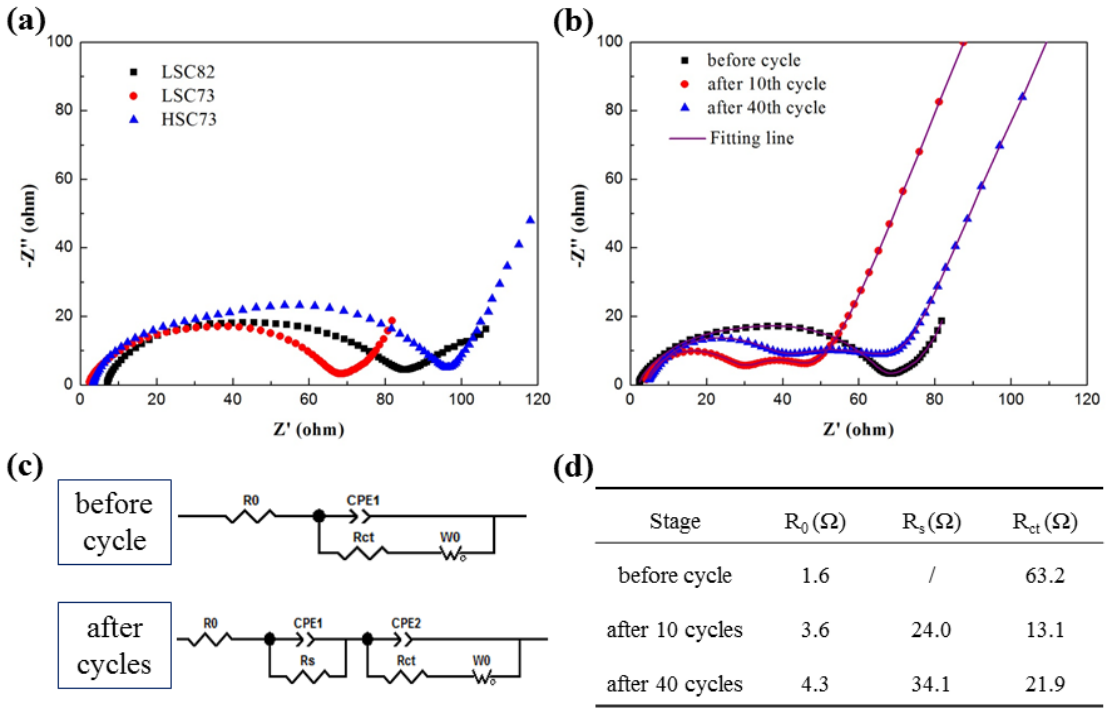

(d)

Stage	R_0 (Ω)	R_s (Ω)	R_{ct} (Ω)
before cycle	1.6	/	63.2
after 10 cycles	3.6	24.0	13.1
after 40 cycles	4.3	34.1	21.9

Figure 5. Nyquist plots of S/HCF cathodes: (a) comparison among different composite cathodes; (b) LSC73 cathode before and after cycles; (d) resistance data of LSC73 cathode fitted from (c) the equivalent circuit.

To further realize the role of HCF in promoting cell performance, the structure variation of LSC73 cathode during cycling was recorded. As shown in Fig. 6a, the cathode presents a porous

morphology before cycle, which favors convenient ion transport in the electrode. After cycles, plenty of insoluble deposits are closely attached by the fiber chain on the electrode (Fig. 6b). In other words, the conductive network fabricated by the cross linked nanofibers provides sufficient deposition positions for the reaction byproducts. Meanwhile, the porous electrode could have certain adsorption ability towards these sulfide species. Therefore, the possibility of active material separating from conductive region is reduced [18] and the irreversible capacity loss is controllable. Besides, the fiber framework remains intact on the whole over repeated cycles owing to its good mechanical properties, thus the volume expansion of the cathode can be withstood.

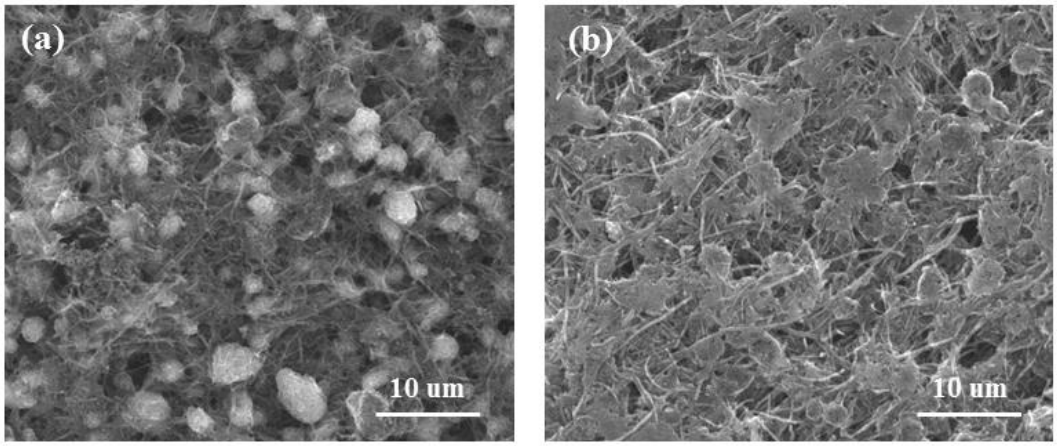

Figure 6. SEM images of LSC73 cathode (a) before cycle and (b) after cycles

4. CONCLUSIONS

Unique structured sulfur-hollow carbon nanofiber composites were prepared and applied for the cathode of Li-S batteries. The preparation method and S content have remarkable influences on the structure and properties of the composite. Severe agglomeration and large-sized particles easily arise in the composite by heat treatment process, while the liquid precipitation route promotes the formation of smaller spherical particles and better S/C distribution. The HCF can contact compactly with S under strong combination force if S content is appropriate in the composite. An initial capacity of 1165 mAh g^{-1} and capacity retention of 75.7 % after 40 cycles (based on second discharge) are exhibited in the case of LSC73 cathode. The novel one-dimensional hollow carbon nanofiber material exhibits a promising application prospect for high performance Li-S batteries.

ACKNOWLEDGEMENTS
This work was financially supported by Natural Science Basic Research Plan in Shaanxi Province of China (No.2016JQ5040).

References

1. Z. Lin, C. Liang, *J. Mater. Chem.* A, 3 (2015) 936-958

2. A. Manthiram, Y. Fu, S. H. Chung, C. Zu, Y. S. Su, *Chem. Rev*., 114 (2014) 11751-11787
3. J. Liang, Z.-H. Sun, F. Li, H.-M. Cheng, *Energy Storage Materials*, 2 (2016) 76-106
4. N. Moreno, A. Caballero, L. Hernán, J. Morales, *Carbon*, 70 (2014) 241-248
5. L. Zeng, F. Pan, W. Li, Y. Jiang, X. Zhong, Y. Yu, *Nanoscale*, 6 (2014) 9579-9587
6. X. Gao, J. Li, D. Guan, C. Yuan, *ACS Appl. Mater. Interfaces*, 6 (2014) 4154-4159
7. N. Brun, K. Sakaushi, L. Yu, L. Giebeler, J. Eckert, M. M. Titirici, *Phys. Chem. Chem. Phy*., 15 (2013) 6080-6087
8. J. Chen, Q. Zhang, Y. Shi, L. Qin, Y. Cao, M. Zheng, Q. Dong, *Phys. Chem. Chem. Phy*., 14 (2012) 5376-5382
9. Q. Li, Z. Zhang, K. Zhang, J. Fang, Y. Lai, J. Li, *J. Power Sources*, 256 (2014) 137-144
10. K. Zhang, Q. Zhao, Z. Tao, J. Chen, *Nano Res*., 6 (2013) 38-46
11. X. Cui, Z. Shan, L. Cui, J. Tian, *Electrochim. Acta*, 105 (2013) 23-30
12. J. Yang, J. Xie, X. Zhou, Y. Zou, J. Tang, S. Wang, F. Chen, L. Wang, *J. Phys. Chem*. C, 118 (2014) 1800-1807
13. L. Zhou, X. Lin, T. Huang, A. Yu, *Electrochim. Acta*, 116 (2014) 210-216
14. Y.-S. Su, A. Manthiram, *Electrochim. Acta*, 77 (2012) 272-278
15. H. Lu, Y. Yuan, K. Zhang, F. Qin, Y. Lai, Y. Liu, *J. Electrochem. Soc*., 162 (2015) A1460-A1465
16. H. Lu, Y. Yuan, Z. Hou, Y. Lai, K. Zhang, Y. Liu, *RSC Adv*., 6 (2016) 18186-18190
17. J. Li, F. Qin, L. Zhang, K. Zhang, Q. Li, Y. Lai, Z. Zhang, J. Fang, *J. Mater. Chem*. A, 2 (2014) 13916-13922
18. Y. Diao, K. Xie, X. Hong, S. Xiong, *Acta Chim. Sinica*, 71 (2013) 508-518